CHAPTER 3

Cam-follower system

"Every scientific truth goes through three stages.
First, people say it conflicts with the Bible.
Next they say it had been discovered before.
Lastly, they say they always believed it."

Louis Agassiz (1807-1873)

In the present chapter the complex behaviour occurring in a class of impacting mechanical systems is investigated. Specifically, we have studied a simplified model of an automotive camshaft system. This system can be modeled as a forced impact oscillator and gives rise to a variety of dynamics that makes worth its study. In particular, several nonsmooth phenomena as first detachment, transition from complete to uncomplete chattering, discontinuity-induced bifurcations of periodic orbits can be exhibited. We will analyse these complex behaviours under variations of the rotational speed of the cam. Once we have observed the different behaviours occurring in our system, we will state analytical explanations of all the nonsmooth phenomena mentioned before.

3.1 Introduction

The modeling and analysis of multi-body mechanical systems is one of the corners stones in modern mechanical engineering [22, 135]. In particular, systems that involves impacts (and friction) have been of special interest, since most systems are affected by their presence (see [20, 23, 100]). To

model a mechanical system it is important to have a clear idea of what material properties the different components that make up the mechanism have. This is particularly important when modeling impacts, since different impact models resembles different material properties (see *e.g.* [21]). In this chapter we will assume that all components are rigid and that impacts occur instantaneously, *i.e.* in zero time.

Mechanical systems with rigid bodies are often modeled as systems of second order *ordinary differential equations* (ODEs). The dynamical behaviour of the model can then found by solving the ODEs. Only very simple systems of ODEs can be solved explicitly [6], but more commonly the ODEs have to be solved using some numerical method [8, 7]. Furthermore, systems with impacts fall into a wider group of systems that are often referred to as *nonsmooth* (NS) or *piecewise smooth* (PWS) systems. In recent years there have been a lot of analysis and research into NS systems. The research has spanned from proving uniqueness and existence of certain trajectories [86] to the effects of low-velocity impacts (so-called *grazing impacts*) [109]. To further complicate things there are, at least, three different popular approaches to deal with NS systems, the *complementarity system* approach [24, 82], the *differential inclusion* approach [9] and the *hybrid system* approach [90]. The different approaches have shown to be good for different purposes and depending of what the goal with the analysis have been. In the present chapter we will use the third approach, the hybrid system approach, where a system of second order ODEs is rewritten as a system of first order ODEs and where smooth dynamics is accompanied with discrete maps at *discontinuity surfaces*. A discontinuity surface could for instance be a rigid wall against which another rigid object is impacting. The hybrid system approach has shown to be particularly successful when trying to understand and explain qualitative dynamical changes caused by the interaction of invariant sets, such as limit cycles, and discontinuity surfaces [92]. Such dynamical changes is referred to as *discontinuity induced bifurcations* (DIBs) and differs from the bifurcations that can be found in standard smooth dynamical systems [96]. See [55] for a more thorough discussion about DIBs.

In addition, the hybrid system approach has also been useful when it comes to stability and bifurcation analysis of limit cycles and continuation of limit cycles and DIBs of limit cycles. Especially, the introduction of *discontinuity mappings* [108] has made it possible to analyse local behaviour of DIBs.

In this chapter we will analyse a system that resembles that of a real

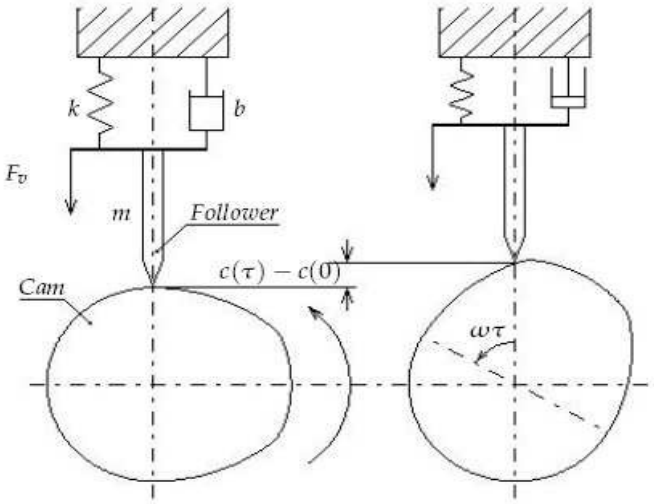

Figure 3.1: Cam-Follower schematics. *(a)* t=0 *(b)* t=τ.

cam-follower system and show some of the characteristic dynamical features that the real systems sometimes show. Cam-follower systems can be found in most modern engines and there is a plethora of different approaches in which these systems are modeled [112]. In Fig. 3.1 we show a schematic of the cam-follower system that will be analysed in this chapter. During normal working conditions the tip of the follower is always in contact with the cam and thus the piston is moving regularly up and down. However, sometimes when the cam is rotating with a high frequency the follower can release from the cam and then bounce against the cam until it comes to rest through an accumulation of impacts. Such accumulation of impacts is sometimes referred to *Zeno behaviour* [151] or *chattering* [25] and can make the engine less effective and cause wear problems. A possible reason for follower release is the shape of cam. It is not uncommon to produce cam profiles such that the corresponding acceleration felt by the follower is nonsmooth [112]. See further sec. 3.2 for a discussion about cam profiles. Therefore, technical solutions in order to ensure permanently the contact between the elements are needed. Basically, the contact can be ensured in two ways: by shape or by force [105]. In the first case, solutions as cams with channel (groove) or cams with slot/notch are used. Even though these cams ensure the contact between cam and follower, they also lead to increase the manufacturing cost due to the high execution precision im-

plied. The other way to ensure the contact is to introduce forces or exterior moments generated with help of spiral or helical springs connected to the follower that always pushes the follower against the cam. But depending on the size of the spring force and how big the discontinuous acceleration change is the follower can leave the cam for some time anyway.

Since we will assume all components to be rigid we will use a standard *Newton restitution law* at impacts. The effect of this is that we will have the possibility of chattering every time the follower releases from the cam. Therefore the main attention in this chapter will be on DIBs the are connected with chattering and the discontinuous acceleration mentioned above. However, we will also analyse other DIBs that can occur in our cam-follower system and explore the mechanisms behind them.

The reminder of this chapter is organised as follows. In Section 3.2 a general introduction to cam-follower systems is done and the specific model that will be analysed in this chapter is defined. In Section 3.4 we introduce the numerical methods that have been used for the numerical analysis. Then in Section 3.5 we will introduce and explore some operating dynamics, causes of follower detachment, chattering, accumulation points, limit cycles, some bifurcation scenarios, and coexistence of attractors. Some of these behaviours are analysed mathematically in Section 3.6. Finally in Section 3.7 we summarise our findings, draw some conclusions and take a look into possible future research.

3.2 Cam Follower Systems: Mechanical modeling.

The formulation of an appropriate mechanical model can be a challenging task for most applications. For cam-follower systems, various models with different complexity have been extensively studied, ranging from models with 1 [89] to 21 Degrees Of Freedom (DOF) [128](by using the additional DOF to include the effects of camshaft torsion and bending, backlash, squeeze of lubricant in bearings etc.). Despite the different possibilities, there is general agreement confirmed by experiments, that a lumped parameter single DOF model is adequate to represent most of the aspects of the dynamic behaviour [18, 89, 3, 56].

Following this approach, we will consider a single DOF model in order to study the dynamical behaviour of cam-follower systems. A schematic diagram is shown in Fig. 3.1. Then, let us consider the model given by the following second order equation to model the free-body dynamics of the

follower

$$m\ddot{q}(t) + b\dot{q}(t) + kq(t) = -mg, \quad if\ q(t) > c(t). \tag{3.1}$$

where m, b, k and g are constant parameters for the follower mass, friction viscous damping, spring stiffness and the gravitational constant, respectively. The state of the follower is given by the position $q(t)$ and velocity $\dot{q}(t)$. The follower motion is constrained to a space region $c(t)$ (see Fig. 3.1). The dynamic behaviour when impacts occurs (i.e. $q(t) = c(t)$) is modeled via Newton's impact law as

$$\dot{q}^+(t) = (1+r)\dot{c}(t) - r\dot{q}^-(t), \quad if \quad q(t) = c(t). \tag{3.2}$$

where $\dot{q}^+(t)$ and $\dot{q}^-(t)$ are the post- and pre-impact velocities, respectively, $\dot{c}(t)$ is the projection of the cam velocity vector at the contact point on the direction of free movement for the follower, and $r \in [0,1]$ is the restitution coefficient to model from plastic to elastic impacts. The Newton's restitution law for modeling of impacts is widely used in engineering given that is sufficient to describe the essential features of the solutions.

Considering the free-body dynamics of the follower governed by eq. (3.1), it is possible to find explicit expression for the solutions of this equation with $q_0 = q(0)$ and $\dot{q}_0 = \dot{q}(0)$ being the initial position and velocity of the follower, respectively. The free-body dynamics is fully described by the following expressions

$$\mathbf{x}(t) = e^{-\zeta t}\left(\mathbf{I}\cos(\omega_s t) + \mathbf{A}\sin(\omega_s t)\right)\mathbf{x_0} \tag{3.3}$$

where,

$$\mathbf{x}(t) = \begin{bmatrix} q(t) \\ \dot{q}(t) \end{bmatrix} + \frac{g}{\omega_0^2}\begin{bmatrix} 1 \\ 0 \end{bmatrix},\ \mathbf{x_0} = \begin{bmatrix} q_0 \\ \dot{q}_0 \end{bmatrix} + \frac{g}{\omega_0^2}\begin{bmatrix} 1 \\ 0 \end{bmatrix},\ \mathbf{I} = \begin{bmatrix} 1 & 0 \\ 0 & 1 \end{bmatrix},$$
$$\mathbf{A} = \begin{bmatrix} \frac{\zeta}{\omega_s} & \frac{1}{\omega_s} \\ -\frac{\omega_0^2}{\omega_s} & -\frac{\zeta}{\omega_s} \end{bmatrix},\ \zeta = \frac{b}{2m},\ \omega_0 = \sqrt{\frac{k}{m}},\ \text{and}\ \ \omega_s = \sqrt{\omega_0^2 - \zeta^2}.$$

In what follows, we will consider the following parameter values [1]: $g = 0$ ms^{-2}, $m = 1.221\ Kg.$, $k = 146 \cdot 9.8\ Kg./s^2$, $b = 0\ Kg./s$, and $r = 0.8$.

The design process for a cam-follower system is a trade off between several optimality criteria usually determined by the application and the restrictions imposed by the physical implementation. The choice of a cam geometry with a discontinuous derivative in its lift profile is frequently found on engineering application [112].

[1] We have considered a gravity equal to zero in order to simplify the calculations but there is no qualitative changes for doing this assumption.

The camshafts on some car engines are cut with a three-dimensional profile that varies along the length of the cam lobe. At one end of the cam lobe is the least aggressive cam profile, and at the other end is the most aggressive. The shape of the cam smoothly blends these two profiles together. A mechanism can slide the whole camshaft laterally so that the valve engages different parts of the cam. The shaft still spins just like a regular camshaft – but by gradually sliding the camshaft laterally as the engine speed and load increase, the valve timing can be optimized.

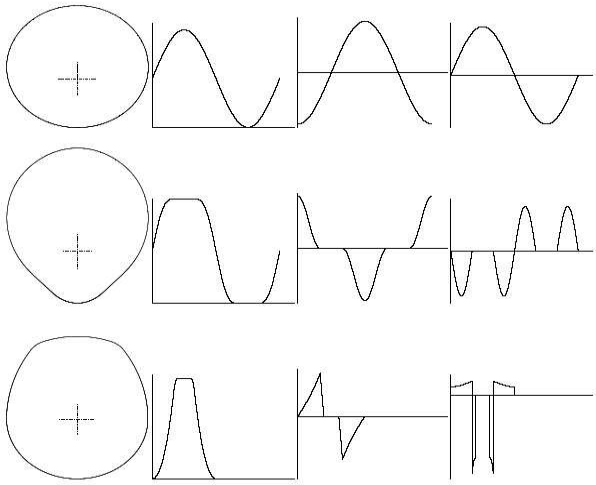

Figure 3.2: Three different cam profiles. From left to right: Cam profiles, Constraint positions, Velocities and Accelerations.

In this work we will use the lift profile with a discontinuous second derivative (case (c) shown before) given the characteristics of a geometric based design process. Fig. 3.3 shows the shape of the cam and the correspondent descriptive function for the position, velocity and acceleration. In what follows we will denote by a, b, c, d, e and f the six points in the cam position where the second derivative is discontinuous (see Fig. 3.3 (b)). Then, we will consider the regions A_1, A_2, A_3, A_4, A_5 and A_6 as the regions between the points (a, b), (b, c), (c, d), (d, e), (e, f) and (f, a) respectively.

The analytical function for the position, velocity and acceleration of the cam profile can be deduced from figure 3.3. Considering the angles θ_1, θ_2 and θ_3 as

$$\theta_1 = \angle SOA \quad \theta_2 = \angle SOB \quad \theta_3 = \angle SOC$$

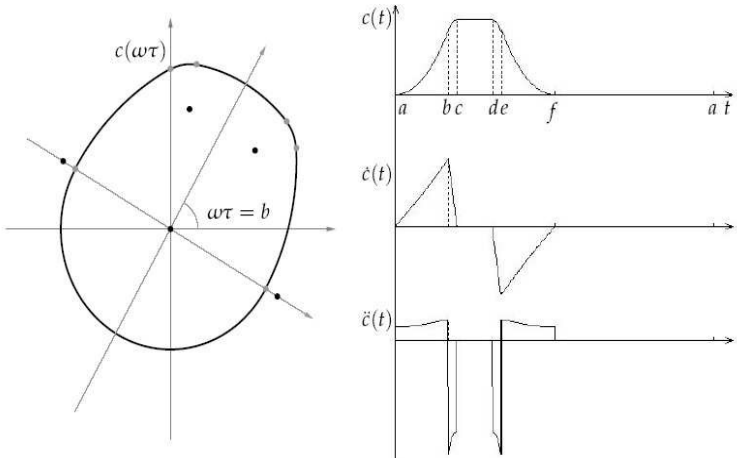

Figure 3.3: (a) Cam profile definition. (b) Constraint position $c(t)$, velocity $\dot{c}(t)$ and acceleration $\ddot{c}(t)$.

the shape of the cam is described by

$$c(\theta) \quad = \quad \begin{cases} c_0(\theta) & \text{If } 0 < \theta \leq \frac{\pi}{2} - \theta_1 \\ c_1(\theta) & \text{If } \frac{\pi}{2} - \theta_1 < \theta \leq \frac{\pi}{2} - \theta_2 \\ c_2(\theta) & \text{If } \frac{\pi}{2} - \theta_2 < \theta \leq \frac{\pi}{2} - \theta_3 \\ c_3(\theta) & \text{If } \frac{\pi}{2} - \theta_3 < \theta \leq \pi \end{cases} \tag{3.4}$$

where $\theta = \omega t + \theta_0$ **mod** 2π, (where θ_0 is the initial phase of the cam). Then, the relation between $c(t)$ and $c(\theta)$ is given by

$$c(t) = c(\theta), \quad \dot{c}(t) = \omega \cdot \dot{c}(\theta), \quad \ddot{c}(t) = \omega^2 \cdot \ddot{c}(\theta). \tag{3.5}$$

In what follows, the cam shape is described by the following functions

$$c_0(\theta) = \rho_0 \tag{3.6}$$
$$c_1(\theta) = -\kappa_1 \sin(\theta + \theta_1) + (\rho_1^2 - \kappa_1^2 \cos(\theta + \theta_1)^2)^{\frac{1}{2}} \tag{3.7}$$
$$c_2(\theta) = \kappa_2 \sin(\theta + \theta_3) + (\rho_2^2 - \kappa_2^2 \cos(\theta + \theta_3)^2)^{\frac{1}{2}} \tag{3.8}$$
$$c_3(\theta) = \rho_3 \tag{3.9}$$

where κ_i and ρ_i are constant parameter given by our particular geometrical construction of the cam as (see Fig. 3.4)

$$\begin{array}{lll} \kappa_1 = \|\overline{OO_1}\| & \rho_0 = \|\overline{OA}\| & \rho_2 = \|\overline{O_2B}\| \\ \kappa_2 = \|\overline{OO_2}\| & \rho_1 = \|\overline{O_1A}\| & \rho_3 = \|\overline{OC}\| \end{array} \tag{3.10}$$

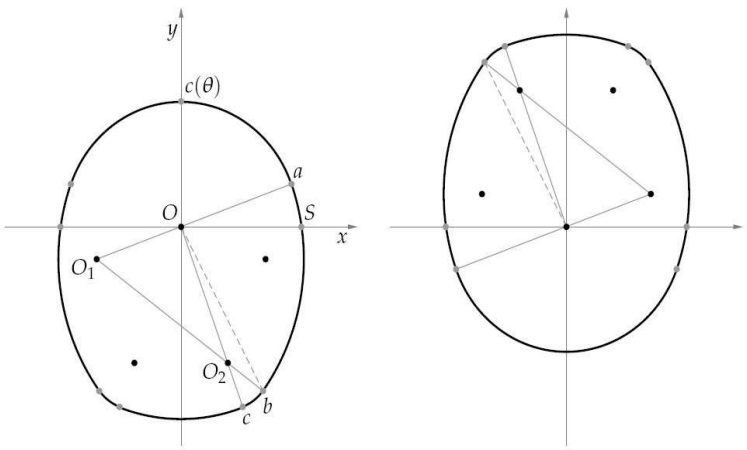

Figure 3.4: Cam profile definition (a) $\theta = 0$ (b) $\theta = \pi$.

The numerical simulations and analytical calculations are performed with the following parameter values: $\kappa_1 = 0.45\ m.$, $\kappa_2 = 0.40393320723821\ m.$, $\rho_0 = 0.1\ m.$, $\rho_1 = 0.85\ m.$, $\rho_2 = 0.55393320723821\ m.$ and $\rho_3 = 0.2539332072\ m.$.

3.3 Notation for periodic orbits

In this chapter, the following notational convention for periodic orbits will be in force. We define globally a Poincaré map (or stroboscopic map), sampling the flow at $t = T = 2\pi/\omega$. Namely, we consider

$$\begin{aligned} P : \mathbb{R}^2 \times \mathbb{R} &\rightarrow \mathbb{R}^2, \\ P : (X_0, t_0) &\rightarrow P(X_0, t_0) = \phi_T(X_0, t_0). \end{aligned}$$

where ϕ_t is the flow generated by the solutions of the system. Let $\Gamma = \{P^k(X_0, t_0)\ \forall k \in \mathbb{Z}, \exists (X_0, t_0)\}$. For $m \geq 1$, we will say that Γ is a mT-periodic orbit iff m is the smallest positive integer for which $(X_0, mT+t_0) = P^m(X_0, t_0) = \phi_{mT}(X_0, t_0)$.

It is relevant to point out that the structure of the stroboscopic map changes according to the number of impacts and we may define different problems for periodic orbits. Thus, if $m \geq 0$ and $s_i \geq 0$, $i = 1, \ldots, m$, we

define

$P(m; s_1 : s_2 : \ldots : s_m) = \{$ mT-periodic orbits with s_i impacts in the period i$\}$

We define $s_i = \infty$ if the trajectory has a chatter motion in the period i, and $s_i = 0$ if there are no impacts or the orbit is sticking during the period.

3.4 Numerical methods.

As mentioned in sec. 3.1 under some circumstances (e.g. if small linear systems are considered) it is possible to find explicit expressions for the solutions of the ODE that describe the free-body dynamics. However, here we use a hybrid system approach, where integrations of smooth ODEs are mixed with discrete maps and vector field switches. In practice, it means that an initial value problem is solved for until the trajectory reaches one of the predefined discontinuity surfaces, where an event occurs. At such a point the vector field is switched and/or the state vector is changed through an impact map and a new initial value problem is solved.

Compared with many other articles on impacting system that uses the hybrid systems approach we do not avoid the numerical problems that chattering (or Zeno behaviour) possesses, but instead we are using a recently developed method (see [111]) to deal with this very specific situation. The main idea with this method is to introduce a *chatter map* that maps the state forward in time when the impacts are accumulating. This means that every time there is an impact and the relative acceleration between two bodies are negative the method checks whether the chatter map can be applied. The method also makes sure that the map does not introduce a bigger error than some tolerance given by the user. After the chatter map has been applied the two object that were impacting each other will now be in contact until the relative acceleration between the two objects becomes positive.

Furthermore, if the hybrid system approach is used it is straightforward to calculate the different types of bifurcation diagrams presented in sec. 3.5.

Finally, in this chapter we have chosen MATLAB's ODE solvers (and mainly RK45, which is a fourth order Runge-Kutta method) with the built-in event location routines to detect the crossings of the discontinuity surfaces. Such event location routines find the zero of the specified functions called *event functions* and the direction of the zero crossing. The values of the relative and absolute tolerance that we have considered to implement

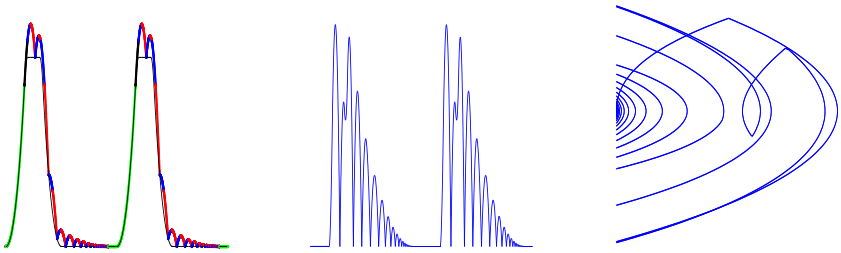

Figure 3.5: Time response for 190 *rpm*. (a) Follower position vs. Cam position. (b) Relative position. (c) Phase space, relative position vs. relative velocity.

the integration method are both 10^{-12}. We have also used a maximum integration step whose value have been 10^{-3}.

3.5 Complex dynamics on cam follower systems

Assuming the cam shape presented in sec. 3.2, the behaviour of our cam-follower system has been computed using the numerical methods described in sec. 3.4. This system define special types of motion. In particular we have that if the cam and the follower come into contact with zero relative velocity and negative relative acceleration, then the follower cannot leave the cam, so it is assumed that *sticking* (or *sliding*) motion takes place until the relative acceleration becomes positive. We also have if the follower is near to the cam and the relative velocity is low, the motion will lead to a rapid series of impacts accumulating in finite time (like a bouncing ball coming to rest) which is termed as *chattering*. After the chattering has completed, sticking motion will follow until the acceleration become positive. Fig. 3.5 shows a typical time response of the follower for 190 revolutions per minute (rpm). Fig. 3.5 (a) represents the follower position versus the cam position. The cam position is displayed using different colors depending on the position and velocity. The green line means a sticking motion. The black line is displayed when the relative acceleration is positive. If the relative acceleration is negative and the relative velocity is positive we represent it with a blue line the points with an increasing relative velocity and with a red one a decreasing relative velocity. As we can see, the response is char-

acterised in this case by a sticking motion and multi-impacting behaviour between the cam and the follower which is well illustrated both in time evolution and phase space diagram reported in Fig. 3.5 (a)-(c).

Cam-follower systems can exhibit different scenarios as periodic orbits with a finite number of impacts in each period, periodic chattering sequences or chaotic attractors. Moreover complex dynamics can be observed under parameters variations as sudden transitions of periodic solutions to chaos, transitions from complete to uncomplete chattering or coexistence of attractors. In the next subsection we will present all these complex behaviours and then, we will try to explain them analytically in Section 3.6.

3.5.1 Observed dynamics

In order to have a better understanding of the dynamical behaviour under parameter variation, we have constructed bifurcation diagrams. Fig. 3.6 (a)-(f) show several brute-force bifurcation diagrams of the cam-follower system under variation of the cam rotational speed. Fig. 3.6 (a),(b),(c),(e) are impact bifurcation diagrams. These diagrams have been obtained by sampling the system states at every impact, and plotting the impact position against each value of the cam velocity. For each value of the cam rotational speed in *rpm*, a fixed initial condition is simulated for a long time in order to be sure that transients have died out and we have plotted for the last 400 periods of the forcing input. In some of the pictures we have represented on the left side the position, velocity and acceleration of the cam.

Fig. 3.6 (d),(f) show stroboscopic bifurcation diagrams. We introduce the stroboscopic map given in Section 3.3. As in the impact bifurcation diagrams we simulate a fixed initial condition for a while, but in this case we plot the last 400 stroboscopic points (the follower position) against the *rpm* parameter. Notice that using brute-force method only can find stable solutions, i.e. unstable solutions are not directly observable.

In Fig. 3.6 (a)-(f) we clearly see the onset of complicated dynamics leading to the sudden formations of seemingly aperiodic solutions and chaos. In particular we are interested in nonsmooth phenomena as first detachment, and nonsmooth bifurcations of periodic orbits. Fig. 3.6(a) shows a nonsmooth phenomena related to the cam speed at which the first detachment occurs near to 114 *rpm*. Before 114 *rpm* the asymptotic dynamic does not include impact because the cam and the follower are always in contact thanks to the restitution force provided by the preloaded spring. After 114 *rpm* a set of period one chattering sequences are generated.

For higher values of cam velocity in region [114,200] *rpm* we can observe that the location of the accumulation point of the chattering sequences varies as function of the cam speed as well as the derivatives of several order. These solutions characterized by the presence of periodic chattering sequences undergo transitions whenever their accumulation point hits the boundary where the cam velocity is non differentiable. This causes transitions to periodic solutions characterized by different impact sequences.

In Fig. 3.6 (a),(b) we observe the destruction of the period one orbit around 198 *rpm*. The structural change in the solution involves the crossing of the accumulation point to the next forcing period. For our parameter values, this implies the generation of a set of period two orbits as a route to chaos.

Fig. 3.6 (c),(d) show the sudden transition from a chaotic attractor to a 3T-periodic solution with eight impacts for the range [357.5,361.5] *rpm*(see the periodicity in figure 3.6(d) and the number of impact in figure 3.6(c)). As we will see below a stable 1T-periodic orbit with two impacts in each period exists in the same region. Then, coexistence of different attractors is given for that region. Moreover, near to 361.2 *rpm*, a nonsmooth transition occurs due to a border-collision of a section of one chaotic attractor with the boundary where the cam profile loses its differentiability. This nonsmooth transition implies the jump of a chaotic attractor to a larger one.

Fig. 3.6 (e),(f) show the complex behaviour for higher values of the cam rotation speed [660,760] *rpm*. In that region it is possible to isolate a stable 1T-periodic orbit with one impact per period that disappears in a process that we call *Corner Impact Bifurcation* CIB. Increasing the cam rotation speed a smooth period-doubling bifurcation takes place. Then, the same CIB phenomena occurs for the period two orbit near to 739 *rpm*, where one of the impacts belonging to the orbit crosses a discontinuity boundary provoking the destruction of the orbit.

3.5.2 Coexistence of Attractors

In order to understand the global behaviour for the region $rpm \in [358, 359]$ a domain of attraction diagram have been simulated using a cell mapping method. The method of cell mapping was developed by Hsu who also provided a detailed mathematical foundation for the technique. This technique reduces the amount of computational work needed to get a reasonably accurate picture of basins of attraction (see [84] for further

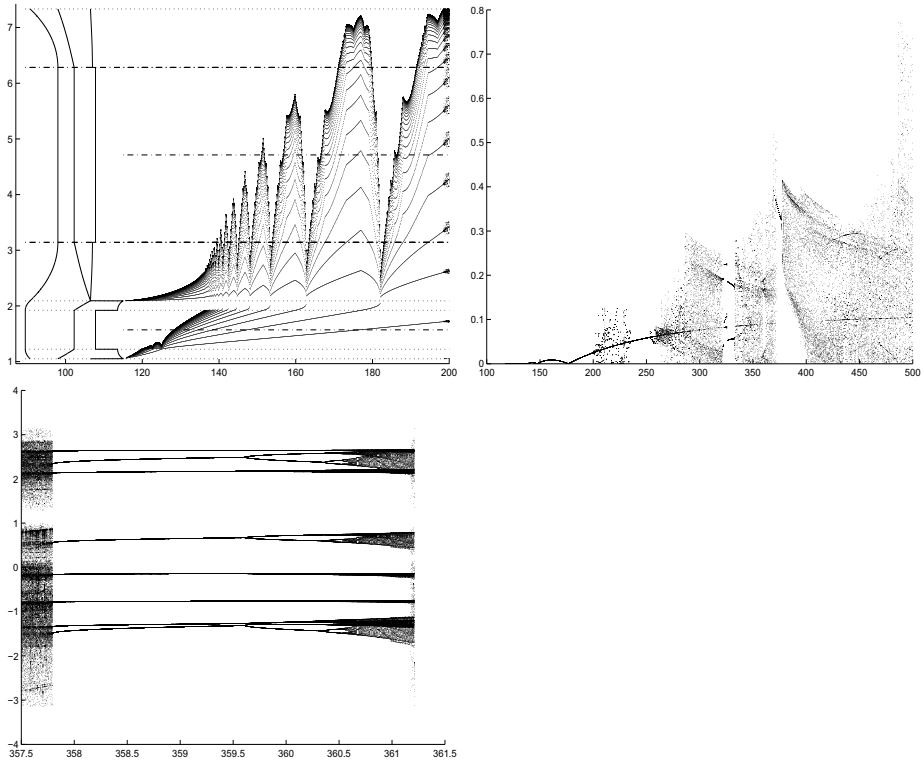
7
6
5
4
3
2
1
100
120
140
160
180
200
0.8
0.7
0.6
0.5
0.4
0.3
0.2
0.1
0
100
150
200
250
300
350
400
450
500
4
3
2
1
0
−1
−2
−3
−4
357.5
358
358.5
359
359.5
360
360.5
361
361.5

given. We have continued two P(1;1) orbits varying the rotational speed. Then, calculating their Jacobian for each value of ω we have explained the corner impact bifurcation presented before. Moreover, we have used the same procedure in order to detect the period-doubling bifurcation. Then, another corner impact bifurcation is explained for the P(2;1:1) orbit.

Finally, we have calculated a domain of attraction diagram in order to show coexisting solutions.

3.6.1 First detachment

As it has been explained before the nominal operating regime of cam follower systems is given by having permanently the contact between the cam and the follower. Therefore an important problem of relevance in application is to assess the onset of complex dynamics due to the detachment between the cam and the follower. It is known that this is an undesirable behaviour and therefore needs to be compensated. In so doing, it is essential to understand the nature of this phenomenon in order to be eliminated or to expand the region of operation of the cam-follower system of interest. In particular, it is important to assess how the system behaves as the rotational speed of the cam is varied.

Considering this, we are interested in the point where the detachment occurs. Let us consider the impact surface, the surface containing all points for which the vector field is tangential to the impact surface, and the intersection between these two surfaces as

$$\Sigma_1 = \{x : H(x) = q(t) - c(t) = 0\},$$

$$\Sigma_2 = \{x : v(x) = \dot{q}(t) - \dot{c}(t) = 0\},$$

and

$$\Sigma_3 = \Sigma_1 \cap \Sigma_2$$

Notice that if the follower device is in contact with the cam they will continue in sticking motion if the relative velocity $v(x)$ (relative to Σ_1) and relative acceleration $a(x)$ (relative to Σ_1) are zero and negative respectively. Therefore the set of detachment points are given by:

$$D = \{x \in \Sigma_3 : a(x) \geq 0\} = \{x \in \Sigma_3 : \frac{d^2}{dt^2}c(t) \leq -w_s^2 \cdot c(t)\}$$

As we can observe $c(t) > 0, \forall t \in \mathbb{R}$, then the only possibility to have detachment is when $\frac{d^2}{dt^2}c(t) < 0$. As it can be seen in the Fig. 3.4, there are two parts, A_2 and A_4, where the cam acceleration holds the condition. For the first part,A_2 it is possible to prove that $a(x), \forall x \in \Sigma_3$ is a monotonic decreasing function. Then, the detachment occurs first in the point where the cam has the first discontinuity in the acceleration (point b) and therefore we just need to solve the equation $a(x) = 0$ for that point. Taking the expression of the cam $c(t)$ and its acceleration $\frac{d^2}{dt^2}c(t)$ given in (3.5) and (3.7) we obtain that the solution is $\omega = 12.041$, $(rpm = 114.979)$ and therefore such value is the rotation speed to obtain the first detachment point in this part. For larger values than $\omega = 12.041$, the set D of detachment points contains more points until to be equal to the region A_2.

For the second part,A_4, it can be proven that $a(x)$ is a monotonic increasing function $\forall x \in \Sigma_3$. Then, the first detachment point should be in the point e, and the rotation speed ω is the same that the calculated value for the first detachment in region A_2, *i.e.*, $\omega = 12.041$. After that, we will have detachment points in an earlier position of the cam for this region when we increase the rotation speed until complete the region A_4. The value of ω in which the set D is equal to the region A_4 is $14.124, (rpm = 134.873)$.

Notice that, in fact for this region, there is no realising in point e for physical reasons because if the system had detachment at that point, the follower must introduce into the cam.

3.6.2 Chattering

Accumulation of impacts is one of many interesting properties of impacting systems. It is possible to distinguish between two different types of impact accumulation, *incomplete chattering* and *complete chattering*. In complete chattering an infinite number of impacts occur in a finite time before the impacting object comes to rest, e.g. a tennis ball that bounces on a table until it comes to stand still. In incomplete chattering, on the other hand, the impacting system almost comes to rest, but after a big number of impacts the relative acceleration between the two impacting objects becomes positive and the relative velocity between the two objects increases during free flight.

In this section we will take a closer look at the transition from complete to incomplete chattering and vice versa.

3.6.2.1 Study of the accumulation points

As can seen in figure 3.8, once the detachment between the cam and the follower occurs we obtain a sequence of chattering in the system. First, the chattering is only in both parts where the cam has a negative acceleration (regions A_2, A_4). But there exists a frequency ω at which the chattering reach the region A_3. We can do some approximations in order to find when exactly the chattering finishes in the upper point (point c). In paper [111] is shown an approximation of first order to simulate chattering in impact systems. If $H(x) = 0$, $v(x) < 0$ and small enough, and $a(x) < 0$, the time it takes for chatter completely is given by

$$\Delta t^* = \frac{1}{1-r}\Big(\frac{2}{a(x)}r\Big)v(x) \tag{3.11}$$

Therefore, we can calculate the rotation speed where the chattering orbit exactly reaches the region A_3. To do that we will take six impacts of the orbit and then we will use the approximation given by (3.11). Each impact gives us a nonlinear equation and the time approximation gives us one more. Therefore, we have a nonlinear system with seven equations and seven parameters. Solving such system in MAPLE we find that the rotation speed ω where the chattering orbit reach the region A_3 is ($rpm = 119.72$).

In figure 3.8 (b) we present the accumulation points of the chattering orbit (green line). In order to calculate such accumulation points we have taken a fixed value of ω, and we have calculated the point before six impacts. And finally, we have used the approximation given by (3.11). As can be seen in figure 3.8 (a), (b), once the orbit has reached the region A_3 we can observe a region of "bubbles" in the bifurcation diagram. Such "bubbles" begin when one of point of the chattering orbit hits the point with the discontinuity in the acceleration of the cam. Then the "bubble" increases at a maximum value and after that it finishes when another point of the chattering orbit hits the point with the discontinuity in the acceleration of the cam.

We have calculated the rotation speed for what one of the impact of the chattering orbit hits the point with the discontinuity in the acceleration. In figure 3.8 we have represented some of this points, the collision of impact points (blue lines) with the discontinuity point. As can be seen some impact of the chattering orbit occurs in the part A_2 and the rest in the other part. For some rotation speed values one of the impacts hits the discontinuity point. An example is considering a rotation speed of $rpm = 120.481$, where five impacts are in the region A_2 and the following hits the discontinuity.

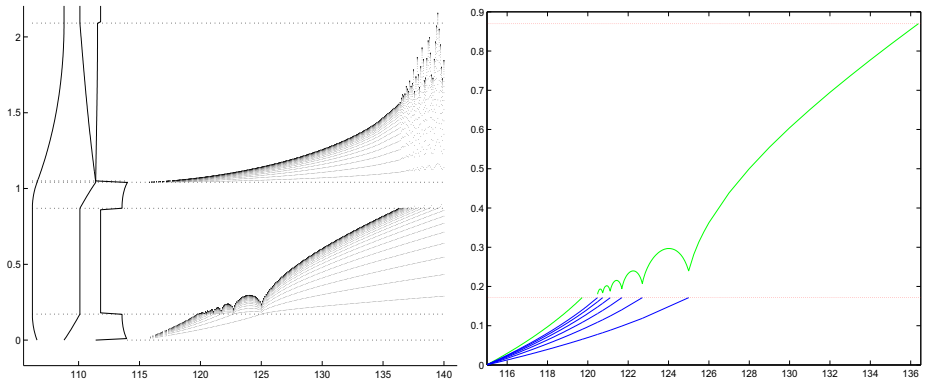

Figure 3.8: Zoom of the first chattering part. (a) Numerical simulation. (b) Analytical calculations

For $rpm = 120.7356$, 121.107, 121.686 and 122.699 we have the collision with the discontinuity and from four to one impacts in the region A_2 respectively. The last collision with the discontinuity for this part is having a direct flight to the discontinuity point. It occurs when $rpm = 124.998$.

Then, increasing ω more than 124.998 the first impact occurs in region A_3 and we have a sequence of complete chattering until the accumulation point arrives at the discontinuity point d ($rpm = 136.38$).

3.6.2.2 Transition from complete to uncomplete chattering

As we can see in figures 3.9(a),(b) around $rpm = 198$ we observe the destruction of the period one chattering sequence around 198 rpm. The structural change in the solution is due to a transition from complete chattering to uncomplete chattering. This transition involves the crossing of the accumulation point to the next forcing period.

In figures 3.9 (a),(b) is shown a time evolution of the cam-follower motion before and after the crossing of the accumulation point. A period one orbit is shown in figure 3.9(a) at $rpm = 198.4$. As we can observe the chattering sequence finishes in a sliding motion (green line) occurs before crossing the next forcing period, and therefore, a complete chattering sequence occurs. When we increase the cam rotation speed, the accumulation point of the chattering sequence reaches is found at the same time that the next forcing period. Then, after that cam rotation speed the chattering

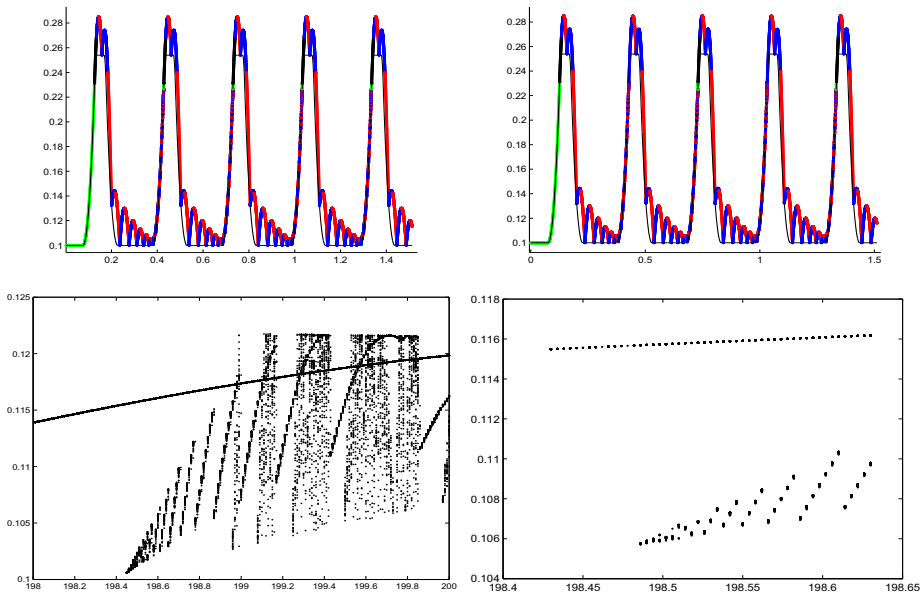

Figure 3.9: Transition from complete to uncomplete chattering. (a) Time evolution for $rpm = 198.4$, (b) Time evolution for $rpm = 198.56$, (c) Stroboscopic bifurcation diagram in range rpm [198,200] (d) Zoom of the stroboscopic bifurcation diagram.

sequence is uncomplete because the accumulation point is in the next forcing period (see figure 3.9(b)). For our parameter values, this implies the generation of a set of period two orbits as a route to chaos. In figures 3.9 (c)-(d) a stroboscopic bifurcation diagram is presented.

3.6.3 Periodic Orbits

In this section we will present a global analysis of the observed periodic orbits, concentrating on the existence of different types of orbits and establishing conditions for the occurrence of one periodic orbits with one impact.

3.6.3.1 Single impact periodic orbits

In this part we will present necessary conditions for the existence of mT-periodic orbits with a single impact. These conditions can be obtained

by constructing the stroboscopic map corresponding to the desired orbit and imposing the periodicity constraint. Let us consider the stroboscopic map at the impact time in order to do easier the calculations. Let $Y(t) = (p(t), q(t))$ be the position and velocity vector of the follower and $Y_{cam}(t) = (c(t), \dot{c}(t))$ for the cam. Considering the impact law given by eq. 3.2, a $P(m; 1:0:\ldots:0)$ is described by

$$Y(0^+) = (Id + R)Y(0^-) - RY_{cam}(0) \tag{3.12}$$

$$Y(mT) = \phi(mT)Y(0^+) \tag{3.13}$$

where

$$R = \begin{pmatrix} 0 & 0 \\ 0 & -(1+r) \end{pmatrix},\ \phi(t) = \begin{pmatrix} cos(w_s t) & \frac{sin(w_s t)}{w_s} \\ -w_s sin(w_s t) & cos(w_s t) \end{pmatrix}$$

and $T = 2\pi/\omega$. Equation 3.12 can now be substituted into the next and taking this into account we obtain:

$$Y(mT) = \phi(mT)SY(0^-) - \phi(mT)RY_{cam}(0) \tag{3.14}$$

where $S = (Id+R)$. Now, by imposing the periodicity constraint $Y(mT) = Y(0^-) = \bar{Y}$ we obtain

$$\bar{Y} = Y(0^-) = -[Id - \phi(mT)S]^{-1}\phi(mT)RY_{cam}(0) \tag{3.15}$$

where the existence of the inverse matrix of $[Id - \phi(mT)S]$ holds for the cases where $\frac{w_s}{\omega} \neq \frac{n}{m}$, for $n = 0, 1, 2, \ldots$.

For the cases in which the inverse matrix exists the initial condition is given by the following expression

$$\bar{Y} = \begin{pmatrix} a \cdot \frac{dc}{dt}(0) \\ -\frac{1+r}{1-r}\frac{dc}{dt}(0) \end{pmatrix}, \tag{3.16}$$

where $a = \dfrac{(1+r)sin(mTw_s)}{w_s(1-r)(1-cos(mTw_s))}$. Moreover, taking into account the impact condition the following equation is hold

$$p(0^-) - c(0) = 0 \tag{3.17}$$

Then, using eq. (3.16) into eq. (3.17) we obtain

$$c(0) = a \cdot \frac{dc}{dt}(0) \tag{3.18}$$

As the condition $c(t) > 0, \forall t \in \mathbb{R}$ is hold, then the impact must be only in regions where $\frac{dc}{dt}(t) \neq 0$. Moreover, due to physical reasons the velocity of the follower just before the impact time $q(0^-) = -\frac{1+r}{1-r}\frac{dc}{dt}(0)$ must be negative. As $r \in [0, 1)$, the impact must occurs in a region where $\frac{dc}{dt}(0) > 0$. Thus, the two possible regions where it is possible to have single impact periodic orbit are A_1, A_2.

Taking all this information into account, the constant a must be positive, and therefore, $sin(mTw_s) = sin(2mw_s/\omega) > 0$. Thus, the region of existence of the single impact mT-periodic orbit ($P(m; 1 : 0 : \ldots : 0)$) is given by

$$\omega > 2mw_s \tag{3.19}$$

and the impact can only occurs in region A_1 or A_2.

3.6.3.2 Continuation of a P(1;1) Orbit

According to the necessary conditions of periodic orbits with single impact, a $P(1; 1)$ may exist with $\omega > 2w_s$. Figures 3.6 (e),(f) represent bifurcation diagrams using a brute force method for the cam-follower parameters considered in the previous sections and $rpm \in [660, 760]$, and a stable P(1;1) impacting in region A_2 is observed in this parameter region. This orbit bifurcates into a P(2;1:1) orbit in a period doubling bifurcation when the parameter rpm is increased. It is also observed that the P(1;1) orbit vanishes as rpm is decreased. This phenomena is due to a corner impact bifurcation as we will show later. The same phenomena occurs to the P(2;1:1) orbit for a $rpm \approx 739.378$. Then, there is a bifurcation from the $P(2; 1 : 1)$ to a chaotic attractor. Moreover, the chaotic attractor has a sudden jump to "larger" chaos when $rpm \approx 740.2$. The impact bifurcation diagram presented in figure 3.12 can provide an explanation about what exactly happen at this point. As shown in a previous section, the chaotic attractor collide with one of the discontinuities in the acceleration and a sudden jump to "larger" chaos is exhibited.

In order to perform a complete scenario we introduce a bifurcation diagram using continuation method in figure 3.10 with the same parameter range. Eq. (3.18) gives us a nonlinear transcendental equation which can be solved numerically in both regions A_1 and A_2 for $\omega > 2w_s$. This equation have been first solved with the package MAPLE, and once a solution has been obtained, it was checked to be of the specified type, since the condition considered is only necessary.

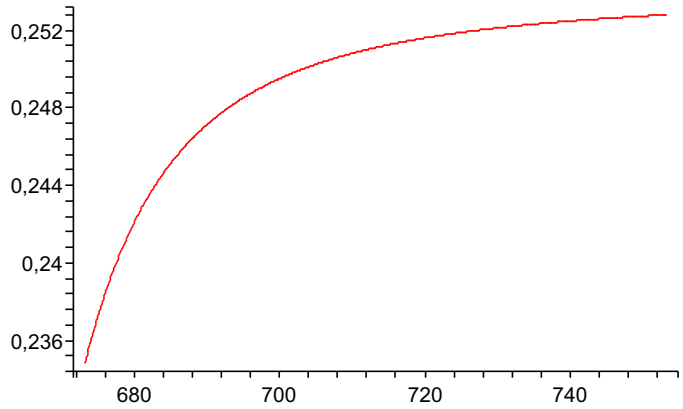

Figure 3.10: Stable P(1,1) bifurcation diagram using a continuation method.

After solving the equation and checking the solution for each region we observe the coexistence of two P(1;1) orbits, one impacting in region A_1 and the other in A_2. Moreover, it can be observed that both P(1;1) orbits exist for every $\omega > 2w_s$ and collide at $\omega = 2w_s$ in a corner impact bifurcation.

For studying the stability of the previously computed $P(1;1)$ we calculate the characteristic multipliers. The characteristic multipliers are computed as follows: we construct the stroboscopic map for the $P(1;1)$ orbit, which is given by:

$$P(Y_0) = \phi(T - t_1)S\phi(t1)Y_0 - \phi(T - t_1)RY_{cam}(t1) \tag{3.20}$$

where Y_0 is the initial condition and t_1 is the impact time. Once we have the stroboscopic map we need to differentiate respect to Y_0 which yields

$$DP(Y_0) = \phi(T - t_1)S\phi(t1) + \frac{\partial P}{\partial t_1}\frac{\partial t_1}{\partial Y_0} \tag{3.21}$$

Then, the characteristic multipliers are eigenvalues of $DP(\bar{Y})$ where $\bar{Y}$ is the initial condition corresponding to the calculated P(1;1) orbit.

In order to calculate $\frac{\partial t_1}{\partial Y_0}$ we will use the impact condition given by

$$p(t_1) - c(t_1) = 0 \tag{3.22}$$

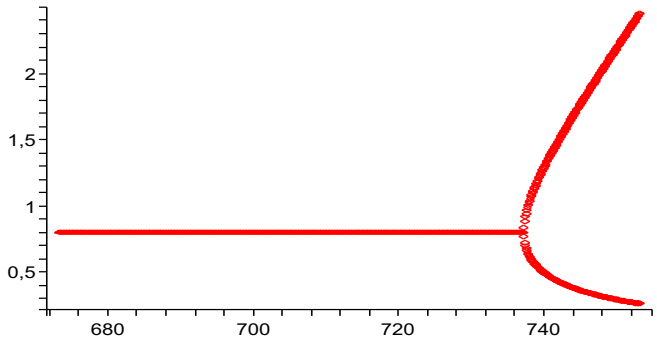

Figure 3.11: Eigenvalues of the stable P(1;1).

Differentiating the left-hand side of this equation with respect to Y_0 and using the implicit function theorem yields

$$\frac{\partial t_1}{\partial Y_0} = -\frac{\phi(t_1)}{\frac{d\phi}{dt}(t_1)Y_0 - \frac{dY_{cam}}{dt}(t1)} \tag{3.23}$$

and we can compute $DP(\bar{Y})$.

In Fig. 3.11 we show the evolution of the characteristic multipliers of the $P(1;1)$ orbits when rpm sweep the range from 672 to 756. For the $P(1;1)$ impacting in region A_1 we observe first that the characteristic multipliers are complex conjugates that move on a circle of radius $r \approx 0.8$, and so the orbit is asymptotically stable. Near $rpm \approx 736$, both characteristic multipliers become real, and when rpm reaches a certain value between $rpm = 736$ and $rpm = 740$ one of the characteristic multipliers has norm greater than 1, and so the periodic orbit becomes unstable. After this point it remains unstable. However, the $P(1;1)$ impacting in region A_2 remains always unstable because one of the characteristic multipliers has norm grater than 1.

3.6.3.3 Analytically Computing the First Period-doubling of a $P(1;1)$ Orbit

Flip and saddle-node bifurcations can be analytically predicted using the stroboscopic map. For example, the first period-doubling bifurcation can be

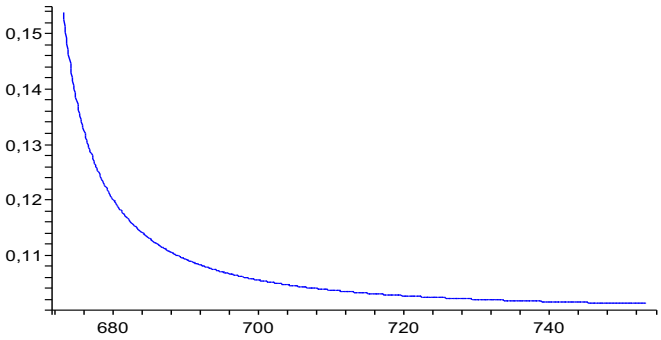

Figure 3.12: Unstable P(1;1) bifurcation diagram using a continuation method.

found as follows: Let $Y_0 = (p_0, q_0)$ be the initial condition for a fixed point by the stroboscopic map P. The eigenvalues of $DP(Y_0)$, or characteristic multipliers, λ_1, λ_2 must be roots of the equation:

$$x^2 - tr(DP(x_0))x + det(DP(x_0)) = 0 \tag{3.24}$$

where tr and det stands for the trace and the determinant respectively. In a period-doubling bifurcation, one of the characteristic multipliers passes through -1, and thus, $DP(x_0)$ must satisfy

$$1 + tr(DP(x_0))x + det(DP(x_0)) = 0 \tag{3.25}$$

Then, imposing the condition for period-doubling 3.25, the condition for the impact 3.13 and the condition for periodicity 3.16, one obtains a system of four nonlinear equations in the unknowns ω, t_1, p_0, q_0, which can be solved with MAPLE. The result in our case:

$$\omega = 739.3197803$$

which is in perfect accordance with the numerical simulations shown in figure 3.12.

3.6.3.4 Analytically computing and classification of corner impact bifurcations

The stability analysis of a periodic orbit in the special case where there is a discontinuity on the second derivative of the lift profile, perfectly fits in the

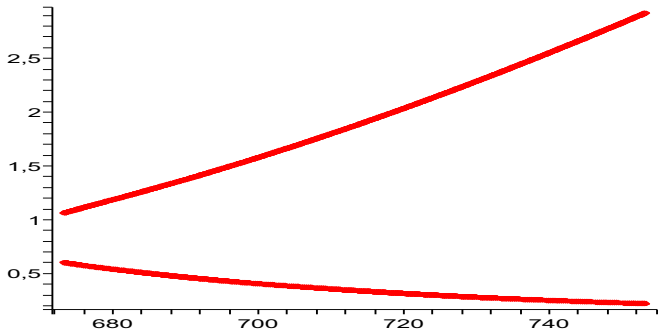

Figure 3.13: Eigenvalues of the unstable P(1,1).

frame of border collision bifurcations of fixed points for two-dimensional piecewise smooth maps [16]. Therefore, we can explain the destruction of the periodic orbit P(1;1) varying the cam rotational speed in what we have called corner impact bifurcation (see [53] for further details).

Considering the impact in point b we can solve equation (3.19) for ω. The point where the corner impact is found at: $\omega \approx 70.50095$ ($rpm = 673.234445$).

To study the structure stability of this periodic orbit we obtain the local map at the bifurcation point, or in other words when the only impact belonging to the orbit hits the discontinuity boundary. Then, calculating the eigenvalues of the Jacobian on the left and right side of the discontinuity we have:

$$\lambda_1^- = 1.0052, \lambda_2^- = 0.6367,$$

$$\lambda_1^+ = 0.68571 + 0.412i, \lambda_2^+ = 0.68571 - 0.412i$$

. At this point we can classify the border collision bifurcation using the methodology presented by Banerjee [16] in which it is used the trace ($\tau^{\pm}$) and determinant ($\delta^{\pm}$) of the Jacobian matrix at each side of the discontinuity boundary. In our case we have

$$\tau^- = 1.6419, \delta^- = 0.64001084, \tau^+ = 1.37142, \delta^+ = 0.8$$

For this particular case we have verified that

$$\tau^- > (1 + \delta^-), \quad \tau^+ < (1 + \delta^+)$$

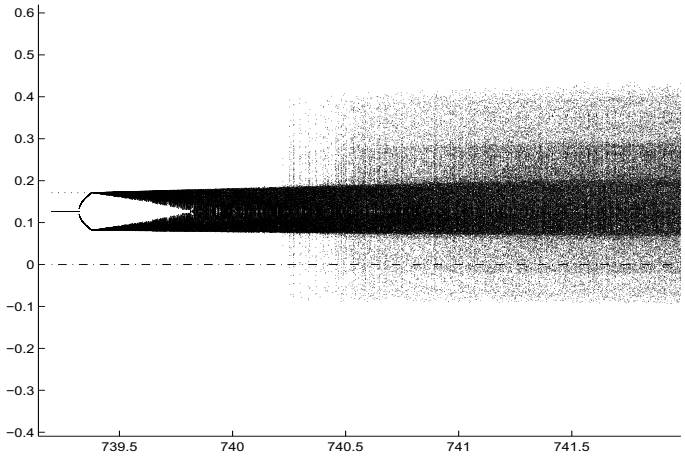

Figure 3.14: Corner impact of the bifurcation of a P(2;1:1) orbit.

Then, the bifurcation scenario we have in Fig. 3.14 is called a *border collision pair* bifurcation, *i.e.*, there is no fixed points on the left side and there are two fixed points on the right side. The two fixed points are born on the border collision bifurcation. More specifically because we also have that

$$(1+\delta^+) > \tau^+ > -(1+\delta^+)$$

then one of the fixed points is stable. Therefore, it is a saddle-node like bifurcation, where a periodic attractor appears at the discontinuity.

Doing the same procedure we can explain the bifurcation occurring at $rpm = 739.37793$ for the P(2;1:1). Calculating the trace and the determinant on the left and right side of the discontinuity we have

$$\tau^- = 1.381624791, \delta^- = 0.4096, \tau^+ = -3.80875, \delta^+ = 0.4096$$

Therefore, it is verified that

$$2\sqrt{\delta^-} < \tau^- < (1+\delta^-), \quad \tau^+ < -(1+\delta^+)$$

In this case the corner impact bifurcation is due to a *border crossing* bifurcation. Then, the scenario we have is a bifurcation from a regular attractor to flip saddle, *i.e.*, a bifurcation from the P(2;1:1) attractor to a chaotic attractor, which is robust.

3.7 Conclusions

In this Chapter the analysis of a cam-follower system have been presented. Specifically, we have studied a simplified model of an automotive camshaft system. This kind of system can be considered as a forced impact oscillator. Therefore, several nonsmooth phenomena as first detachment, transition from complete to uncomplete chattering, discontinuity-induced bifurcations of periodic orbits can be exhibited. We have analysed these complex behaviours under variations of the rotational speed of the cam. Then, in order to have a better understanding of the dynamical behaviour we have constructed bifurcation diagrams. Once we have observed the different behaviours occurring in our system, we have stated analytical explanations of some phenomena. We have calculated the regions with possible detachment points and, particularly, the rotational speed for the first detachment. After the first detachment occurs, we have a sequence of chattering in the system. Then, we have studied analytically the accumulation points of such impacts explaining some phenomena that happen in our system. Another phenomena is the nonsmooth transition from complete to uncomplete chattering. We have observed the destruction of the period one chattering sequence for a certain value of the rotational speed parameter due to the crossing of the accumulation point to the next forcing period. A detailed study of this discontinuity-induced bifurcation is a subject of further research. We have also given necessary conditions for periodic orbits with a single impact. Using these necessary conditions we have continued a periodic orbit of period one and one impact. Such periodic orbit has a suddenly jump to chaos due to a corner-impact bifurcation, and we have been able to explain this bifurcation in an analytical way. Another corner-impact bifurcation of a period 2 orbit is also explained. Finally, coexistence of attractors is shown using domains of attraction calculated with a standard cell-to-cell mapping method.